Song et al. EURASIP Journal on Wireless Communications and Networking (2016) 2016:263
DOI 10.1186/s13638-016-0759-1

EURASIP Journal on Wireless Communications and Networking

RESEARCH Open Access

Modeling link quality for high-speed railway wireless networks based on hidden Markov chain

Jiayang Song*, Huachun Zhou, Wei Quan, Tao Zheng and Ping Dong

Abstract

In high-speed railway (HSR) wireless networks, the link quality is greatly time-dependent and location-varying. Due to the high randomness, it is challenging to predict the link quality in HSR wireless networks. In this paper, we firstly conducted a certain amount of field measurement campaigns of HSR wireless network link quality. A great number of practical datasets are collected regarding packet loss rate (PLR) and round-trip time (RTT). Then, we analyzed its changing pattern in different time scales, and further model the link quality of HSR wireless network using hidden Markov chain. Based on this, an improved algorithm was developed to simulate the variation of HSR wireless network link quality. Simulation results prove that the proposed model is capable of accurately reproducing the behavior of HSR wireless network link quality with regard to PLR and RTT. This work will offer new inspiration to the prediction of link quality for HSR wireless networks.

Keywords: Link quality, High-speed railway, Packet loss rate, Round-trip time, Hidden Markov chain

1 Introduction

High-speed railway (HSR) has brought substantial social and economic benefits. Due to its great superiorities, HSRs are widely built and operated around the world, especially in Europe and East Asia. According to International Union of Railways (UIC), 29792 km of HSR lines had been built by April 2015. With its fast development, the era of HSR has come [1].

Wireless networks play a very important role in the operations of HSR. First, wireless communication is the basis of train operation control systems, which include European Train Control System (ETCS) and Communication-Based Train Control (CBTC) [2]. Second, wireless networks provide great convenience to HSR passengers, such as enjoying multimedia services or online gaming. Emerging wireless technologies have been utilized in HSR. For example, the TD-LTE network of China Mobile had covered 23500 km of high-speed rails by August 2015 [3].

For HSR wireless networks, it is significant to establish reliable wireless links between the trains and the ground. However, the link quality in HSR usually suffers from several sever limitations including complex terrains, Doppler shift. and time-varying channel issue, as discussed in [4, 5].

Recently, many research have been carried out on analyzing the propagation characteristics in typical HSR scenarios, including viaduct, cutting, tunnels, crossing bridges, and stations [5]. In [6–10], the path loss model that considers the height of viaduct and BS antenna were analyzed in viaduct scenario. In cutting scenario, the small-scale fading characteristics were modeled at 2.35 GHz in [11, 12] and at 930 Mhz in [13–16]. In [17], the wave propagation of railway tunnels were analyzed. In [18, 19], the influence of crossing bridges and train stations were reported on propagation loss model. As regards to the measurement frequency, most of the research mentioned above were done at 930 MHz which is the downlink frequency of GSM-R in China. While there exists channel measurement of broadband communication system including WCDMA [20] and LTE [21].

Nevertheless, these research cannot characterize the link quality of wireless networks already deployed along the high-speed rails, so they have limited use in helping improve the performance of existing HSR wireless

* Correspondence: 12111011@bjtu.edu.cn
National Engineering Laboratory for Next Generation Internet Interconnection Devices, Beijing Jiaotong University, Beijing 10044, China

networks. Also, the study on different HSR scenarios cannot provide insight to the global behavior of wireless network link quality of a complete railway line. Hence, modeling the link quality characteristics and its long term pattern of existing HSR wireless networks becomes an issue.

By evaluating the upper layer performance of deployed wireless networks, the variation of wireless link quality along a realistic HSR line can be revealed. In this context, the upper layer is considered as Internet Protocol (IP) layer of protocol stack, whose performance are normally evaluated by parameters of packet loss rate (PLR), round-trip time (RTT).

We reason that PLR and RTT are appropriate parameters to characterize the link quality of HSR wireless networks. First, IP layer performance is the direct reflection of the radio propagation behavior. For instance, a fading channel can result in the loss of signal power that leads to increased bit error rate, which will cause the degradation of PLR and RTT. Second, the wireless channel along the HSR lines varies rapidly, but PLR and RTT are capable of characterizing it. By designing accurate measuring program, we can record the PLR and RTT every 5 s. Besides, since most of the user data in wireless network are IP packets, modeling the IP layer performance directly contributes to the design of novel network architecture.

PLR and RTT are important metrics for wireless communications. In wireless sensor networks (WSN), researchers use PLR to investigate the characteristics of link quality [22] or characterize the information quality [23]. Also, PLR and RTT are proposed as routing metrics for wireless ad hoc networks [24] and wireless mesh networks (WMN) [25]. In the domain of vehicular communication, some research have been conducted using PLR or RTT to design new network architecture [26, 27]. Besides, PLR and RTT are considered as performance indicator for testing commercial platform [28] or evaluating novel communication mechanisms [29–31]. However, no such work was carried out on characterizing the HSR wireless networks link quality using PLR and RTT.

In this paper, we try to model the link quality for HSR wireless networks with PLR and RTT. We firstly conduct a series of field measurement campaigns for PLR and RTT along realistic high-speed rails. The investigation of measurement results reveals a cyclic phenomenon of PLR and RTT. Then we utilize a hidden Markov chain (HMC) reference model to describe the measured PLR and RTT. Based on the model, an improved link quality simulation algorithm is developed. The simulation results prove that the developed algorithm can reproduce the cyclical behavior of PLR and RTT with high accuracy.

The paper is structured as follows: the measurement campaign is detailed in section 2. The investigation of collected datasets is presented in section 3. In section 4, we introduce the HMC reference model. In section 5, an improved link quality simulation algorithm based on proposed HMC model is introduced and evaluated. Section 6 concludes the paper.

2 Measurement campaign

Our measurement campaign was conducted on Beijing–Shanghai high-speed railway in China. In the measurement, the EV-DO (evolution-data optimized) network operated by China Telecom was utilized. The downlink working frequency is 869 MHz–894 MHz, and the uplink is 824 MHz–849 MHz.

During measurement, a dedicated and automated measuring instrument called wireless link monitor (WLM) was produced to measure and store the RTT, PLR, and the corresponding position. The WLM can be considered as a portable industrial computer which has wireless modems connecting to the cellular network along the HSR line. The central processing unit (CPU) of WLM is Intel Core 2 Duo, and the RAM is 2 GB.

As illustrated in Fig. 1, during a period of 5 s, WLM sends ten probe packets to echo server (ES) located on the ground and records the sending time of ith packet as t_i. The size of each probe packet is 64 b, and the interval between two packets is 500 ms. Upon receiving a probe packet, ES sends an echo packet back to WLM immediately. Let P denote the set of echo packets received by WLM within the measurement period, while the number of elements in P is n_{recv}. The receiving time of jth packet is recorded as $t_j^{'}$ where j is the element of P. In a measurement period, PLR is calculated as $n_{recv}/10$, and RTT is calculated by $\frac{1}{n_{recv}}\sum_{j\in P} t_j^{'}-t_j$. Simultaneously, the longitude and latitude of HSR are obtained using a GPS receiver. The measurement results are stored as a quintuple in the database, which are *PLR*, *RTT*, *longitude*, *latitude*, and *time*. The measurement was repeated four times (two round-trips), and four groups of datasets were collected. Each grout consists of more than 120000 entries.

3 Dataset analysis

A statistic analysis was made based on the collected dataset. To reveal the variation behavior of HSR wireless network link quality, a series value of PLR and RTT spanning about 120 min at certain locations are presented in Fig. 2. The value of RTT and PLR are both graded into six intervals, and a single label exhibits the grade of RTT or PLR in a particular position along the railway.

In Fig. 2, it clearly shows that the variation of PLR and RTT approximately present a cyclical phenomenon. In areas *B*, *D*, *F* for PLR and areas *H*, *J*, *L* for RTT, a large part of values of PLR and RTT are relatively low, which

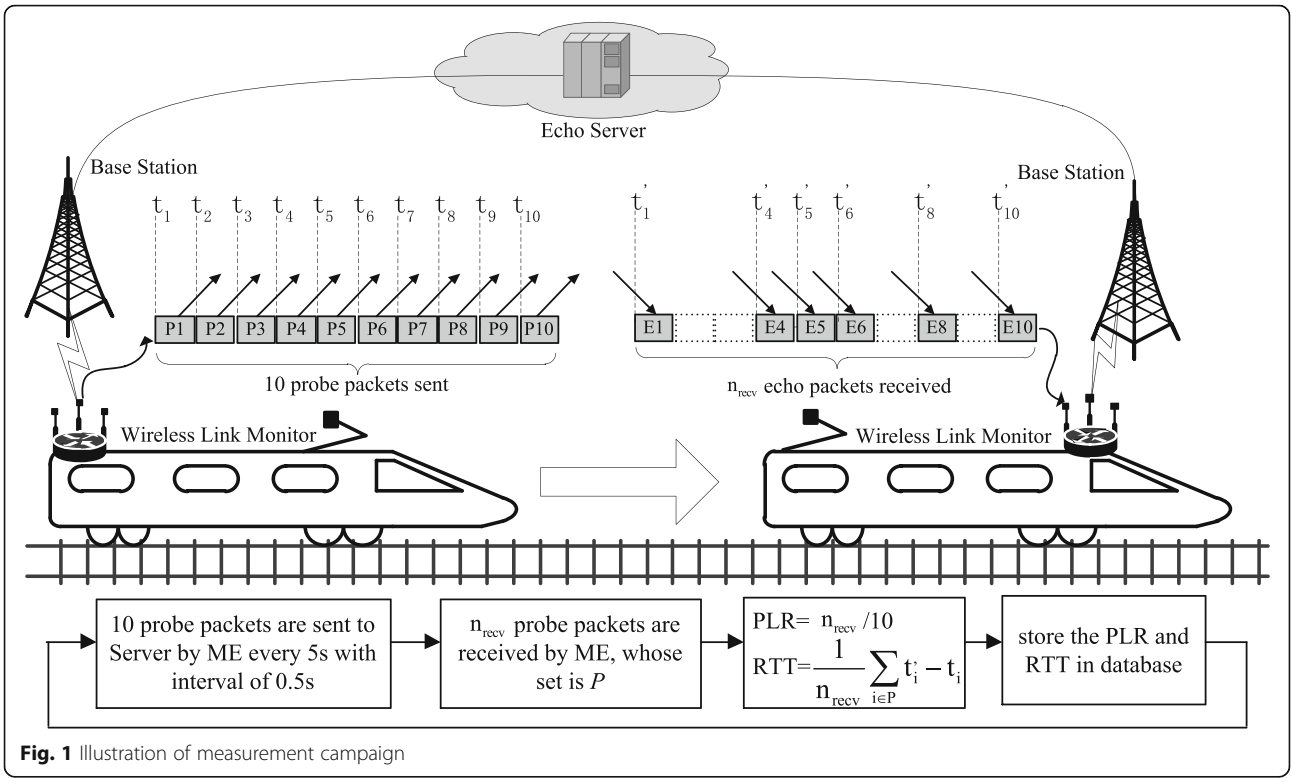

Fig. 1 Illustration of measurement campaign

means that the link quality of HSR wireless networks is in good condition. In contrast, the value of PLR and RTT are rather high in areas *A*, *C*, *E* for PLR and areas *G*, *I*, *K* for RTT, which indicate that the HSR wireless network link quality is under poor condition. The period of good and poor condition appears in turn. Based on the above analysis, we can preliminarily get the first conclusion: the link quality of HSR wireless networks follows a cyclical variation that good condition and poor condition occur alternately.

To further study the cyclical behavior of HSR wireless networks link quality, how the PLR and RTT vary against

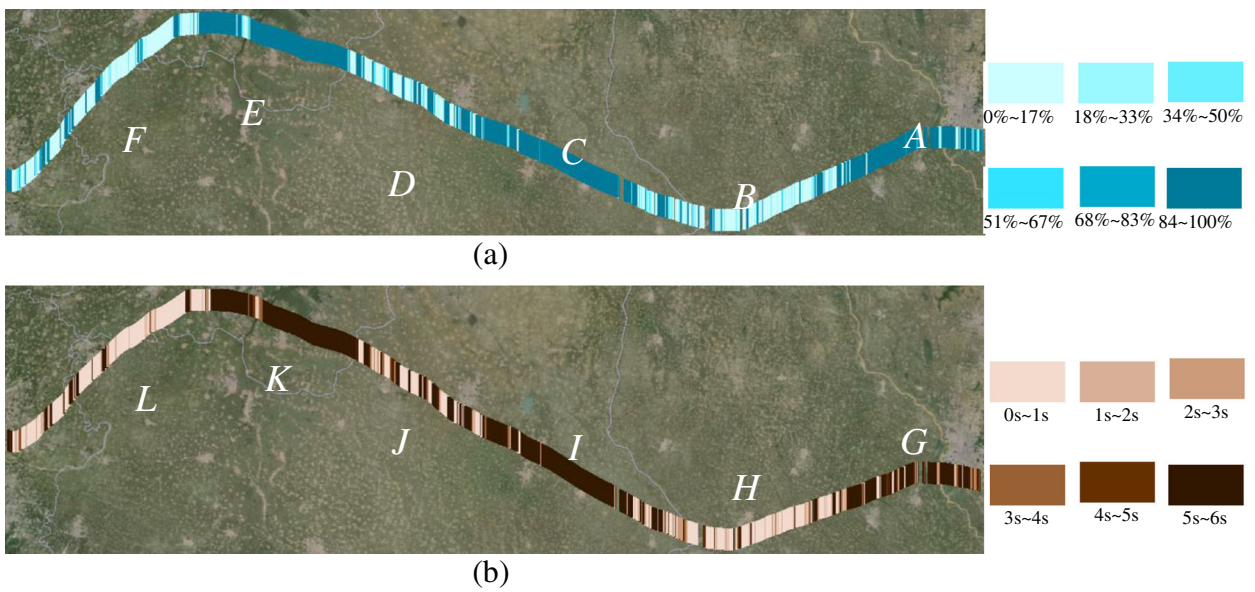

Fig. 2 The measured value of PLR (**a**) and RTT (**b**) at certain locations

time is shown in Fig. 3. The values of measured RTT and PLR are quantized into six states, ranging from *1* to *6*. The percentages of PLR are calibrated as follows: state *6* is given for 83% and above, *5* for 67% ~ 83%, *4* for 50% ~ 67%, *3* for 33% ~ 50%, *2* for 17% ~ 33%, and any lower than 17% is state *1*. The values of RTT are categorized as below: state *6* for 5 s ~ 6 s, *5* for 4 s ~ 5 s, *4* for 3 s ~ 4 s, *3* for 2 s ~ 3 s, *2* for 1 s ~ 2 s, and *1* for 0 s ~ 1 s. In accord with the result from spatial perspective, the values of PLR and RTT also present approximate cyclical variation in time domain. From beginning to 20th minute, 36th minute to 50th minute, and 70th minute to 82nd minute, most of the PLR and RTT states are among *4*, *5*, and *6*. These periods are the counterpart of areas *B*, *D*, *F* for PLR and areas *H*, *J*, *L* for RTT in Fig. 2. On the contrary, from 20th minute to 36th minute, 60th minute to 70th minute, and 82nd minute to 100th minute, PLR and RTT states of *1*, *2*, and *3* happen a lot. These periods are the counterpart of areas *A*, *C*, *E* for PLR and areas *G*, *I*, *K* for RTT in Fig. 2. Hence, we get the second conclusion: among the good condition periods of HSR wireless networks link quality, the states of *1*, *2*, and *3* happen more often. While among poor condition periods, states of *4*, *5*, and *6* occur a lot.

According to the two conclusions mentioned above, the states of HSR wireless network link quality is *controlled* by another variable that cannot be observed. If this invisible variable is in good condition, among the observed states of HSR wireless link quality, *1*, *2*, and *3* occur more often. Otherwise, *4*, *5*, and *6* happen with higher probabilities. We define the observed state of HSR wireless link quality as *micro-state*, whose state space is $Q = \{1, 2, 3, 4, 5, 6\}$. The invisible variable that *controls* the variation of micro-state is defined as *macro-state*. Its state space can be described by $S = \{G, P\}$. *G* is the abbreviation for *good* macro-state, and *P* is for *poor* macro-state.

In Table 1, the measured PLR and RTT values are categorized into *poor* macro-states and *good* macro-states. The criterion used to categorize the dataset is as follows: in a group of PLR or RTT values, if the percentage of micro-states *4*, *5*, and *6* exceeds 75%, then the macro-state of this group is determined as *poor*; otherwise, the macro-state is *good*. We elaborate this criterion according to the careful investigation of results of measurement campaign. The *PLR No.* or *RTT No.* represents serial number of the measured value. Since the PLR or RTT is recorded every 5 s, the *PLR No.* or *RTT No.* can be used to derive the elapsed time since first recorded value.

The frequency of transitions among different macro-states is rather low. As shown in Table 1, during the period of about 1 h, the macro-states of PLR and RTT changed only six times. For *poor* macro-state and *good* macro-state, the minimum duration are, respectively, 540 s and 900 s. Considering that the average operating speed of Beijing–Shanghai high-speed railway is 280 km/h, the shortest distance of *poor* macro-state and *good* macro-state can reach 42 km and 70 km.

4 HSR wireless network link quality modeling

The sequences of PLR and RTT values evolving with time can be interpreted by a random process. To represent it, we introduce a reference model whose random variable possesses two states: macro-state and micro-state, just as PLR or RTT does. The state spaces of macro- and micro-state are, respectively, *S* and *Q*.

In Fig. 4, we use a diagram of the introduced model to illustrate the relationship between micro-states and macro-states. How micro-states are generated is dependent on the macro-state the wireless network link quality undergoes. For example, if the random variable is under the macro-state of *good*, its micro-state takes the values of *1*, *2*, and *3* with higher probabilities. Otherwise,

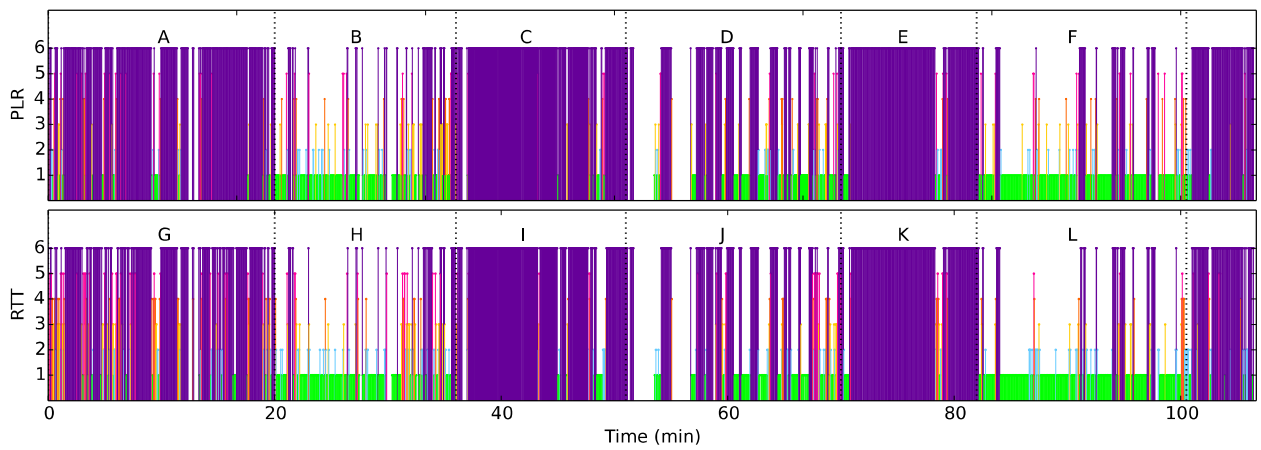

Fig. 3 The measured state of PLR and RTT varying with time

Table 1 Macro-state categorization

Macro-state	PLR No.	RTT No.
Poor	1–391	1–392
Good	392–724	393–674
Poor	725–1454	675–1225
Good	1455–1762	1226–1616
Poor	1763–2029	1617–1851
Good	2030–2356	1852–2208
Poor	2357–2466	2209–2317

micro-states *4*, *5*, and *6* occur more often under macro-state of *poor*. In this figure, solid lines with white arrows indicate that the macro-state transitions from one state to another. We define α_{ij} as the probability that the macro-state transitions from state i to state j in a single step. That is,

$$\alpha_{ij} = P(s_{t+1} = j | s_t = i),\ i, j \in S \tag{1}$$

Dotted lines with black arrows indicate the generation of micro-state under different macro-state. $\beta_s(q)$ is defined as the generation probability that the micro-state q is generated under macro-state s. That is,

$$\beta_s(q) = P(q_t = q | s_t = s),\ s \in S,\ q \in Q \tag{2}$$

The average time interval between different micro-states is much less than that of different macro-states. In other words, the macro-state varies at a much slower pace than micro-state does. According to the results of measurement campaign, every 1053 s on average, the macro-state of HSR wireless network link quality would change. However, the micro-state varies every 5 s, since RTT and PLR were calculated and recorded every 5 s.

For a better understanding of how the proposed model evolves, we introduce an intuitive but simple dice-coin experiment. The experiment is detailed as follows:

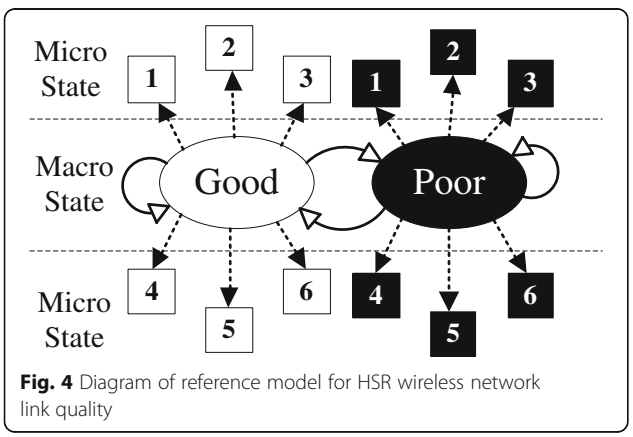

Fig. 4 Diagram of reference model for HSR wireless network link quality

(1) A white-loaded dice whose weight is unevenly distributed. When it is rolled, the probability that one side faces upwards is p_W^i where $i \in \{1, 2, 3, 4, 5, 6\}$. Since the dice is loaded, we define $p_W^m > p_W^n$ for $m < n$.
(2) A black-loaded dice. The face-up probability of one side is p_B^j where $j \in \{1, 2, 3, 4, 5, 6\}$. In contrast with the white dice, we define black dice as $p_B^m < p_B^n$ if $m < n$
(3) A white-loaded coin, the weight of heads and tails are different. P_W^H is the probability that the upper side is heads after tossing it, while P_W^T for tails, and $P_W^H > P_W^T$.
(4) A black-loaded coin. The face-up probability of heads is P_B^H, and tails is P_B^T, while $P_B^H > P_B^T$.

Six sides of the loaded dice represent the six micro-states of HSR wireless network link quality. Rolling white-loaded dice stands for the generation of micro-state under *good* macro-state, while rolling the black dice stands for that under *poor* macro-state. Tossing the loaded coins regulates the variation of macro-state. The white coin represents the transition from *good*, while the black coin represents that from *poor*.

To generate a series of output with the same cyclical behavior possessed by the measured HSR wireless network link quality, the experiment is conducted as shown in Fig. 5:

(1) Randomly select one dice. Roll it, then the first result is generated.
(2) Next, select the coin whose color is identical to the dice rolled at last step. For example, if black dice was just rolled, then the black coin will be flipped.
(3) If the result of coin flipping is heads, continue to roll the dice just rolled before and record the result. Otherwise, roll the other dice.
(4) Go to step (2), until expected number of dice rolling results are recorded.

The rolled dice at every step regulates the generated output sequence, which is similar as the behavior that macro-state of HSR wireless link quality regulates the generation of micro-state. White and black dices are the analogs of the *good* and *poor* macro-state, respectively, while the side of the dice facing upwards represents the generation of micro-state. Hence, we have

$$p_W^i = \beta_G(i), i \in Q \tag{3}$$

$$p_B^j = \beta_P(j), j \in Q \tag{4}$$

Switching between black and white dice, which is regulated by flipping black or white coins, is the analog of

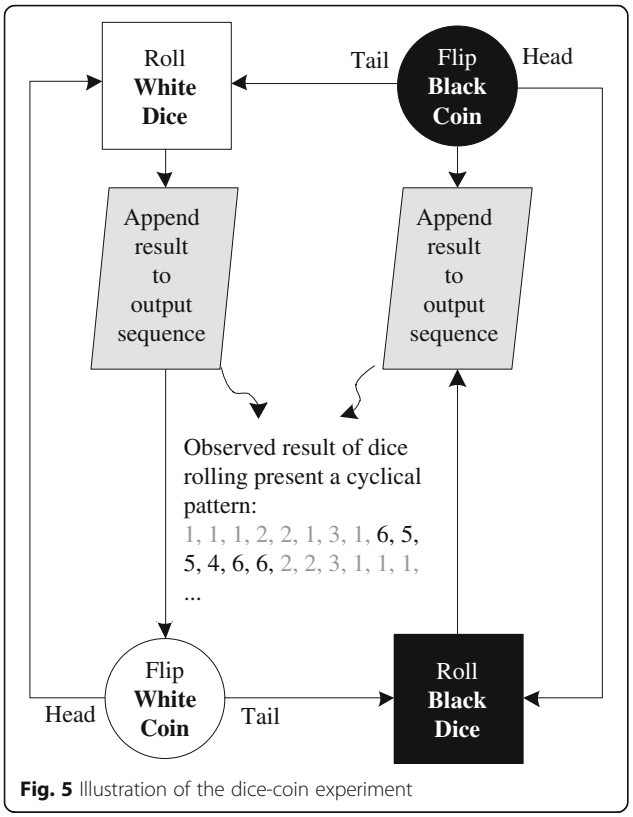

Fig. 5 Illustration of the dice-coin experiment

transition between *poor* and *good* macro-state. The probability of *heads* equals the probability that the macro-state remains unchanged. Similarly, the probability of *tails* is the same as the probability that the macro-state changes. That is

$$P_W^H = \alpha_{GG}, P_W^T = \alpha_{GP}, P_B^H = \alpha_{PP}, P_B^T = \alpha_{PG} \tag{5}$$

Thus, by $P_W^H > P_W^T$ $P_B^H > P_B^T$, the transitions from one macro-state to another one occur less frequently than that to the same one. In the long-term perspective, the macro-state of HSR wireless network link quality may remain unchanged for a certain time.

The dice-coin experiment can generate a series of output results possessing the similar cyclical behavior as the measured PLR or RTT shows. It proves that the proposed reference model can well explain how the cyclical pattern of HSR wireless network link quality evolves.

To further study the cyclical behavior of HSR wireless network link quality, we utilize HMC to describe the introduced reference model. HMC can be considered as a mixture of two stochastic processes [32]. The output of one stochastic process is observable, while the other is not. The observable process is dependent on the unobserved one. In our case, the generation of micro-state and the variation of macro-state can be described by the observable process and unobservable process, respectively.

However, adopting HMC in modeling HSR link quality requires some preconditions. Markov chain concerns with the transition from one state to another, and the transition probability should be stable. In high-speed railway scenario, the stable transition probability can be guaranteed only if the following two preconditions are satisfied: (i) the distance between two base stations is constant; (ii) the speed of the train is constant.

In our measurement campaign, these two preconditions can be fulfilled. Since the dataset used to derive A and B are collected in plain terrain without passing any train stations, the base stations along the corresponding railway line follow an even distribution. Also, the speed of the train is nearly stable during the measurement. But we should note that modeling HSR link quality with HMC is suitable for specific situations where these two preconditions are satisfied. For scenarios such as train stations where the train is speeding up (or slowing down), the proposed model cannot accurately characterize the link quality of HSR.

Normally, HMC can be described using a quintuple. The five elements and their symmetries when utilizing HMC to model HSR wireless network link quality are described as follows:

- S is the state space of the unobserved stochastic process, whose variable is referred to as *state*. In this case, S equals $\{G, P\}$ that is the state space of macro-state.
- Q is the state space of the observable stochastic process, whose element is referred to as *symbol*. In this case, Q equals {1, 2, 3, 4, 5, 6} that is the state space of micro-state.
- A is the state transition matrix. In this case, its element is the transition probability of macro-state, which is α_{ij} shown in Eq. 1.
- B is the symbol generation matrix. In this case, its element is the generation probability of micro-state, which is $\beta_s(q)$ shown in Eq. 2.
- Π is the initial state matrix whose element is the probability of a state with which the unobserved process begins. In our case, it is determined as [0 1], since the macro-states of PLR and RTT both begin with *poor*.

A of PLR and RTT are noted as A_{PLR} and A_{RTT}. In this case, since there are two states, A_{PLR} or A_{RTT} can be defined as a two-by-two matrix. The elements in A_{PLR} and A_{RTT} are derived based on the collected dataset shown in Table 1. Take the first element (α_{GG}) in A_{PLR} or A_{RTT} as an example. α_{GG} is the probability that the state transits from *good* to *good*. Let N1 be the

number of state transitions begin with *good*. Let N2 be the number of state transitions begin with *good* and end with also *good*. Then α_{GG} can be calculated as N2/N1. Note that N1 and N2 can be easily counted from the collected dataset. The rest of the elements of A_{PLR} and A_{RTT} are derived in the same way as α_{GG}.

B of PLR and RTT are noted as B_{PLR} and B_{RTT}. Both of them are defined as two-by-six matrices, since there are six symbols and two states in this case. The elements in B_{PLR} and B_{RTT} are also calculated according to the collected dataset. Take the first element in B_{PLR} or B_{RTT}, which is $\beta_G(1)$, for instance. $\beta_G(1)$ represents the probability that the symbol is observed as 1 when the state is *good*. Let M1 be the number of observations that the state is *good*. Let M2 be the number of observations that the symbol is 1 while the state is *good*. Thus, $\beta_G(1)$ is calculated M2/M1. M1 and M2 can also be counted from the measurement results. The rest of the elements of B_{PLR} and B_{RTT} are derived similarly.

Thus, four matrices of A and B are derived as follows:

$$A_{PLR} = \begin{bmatrix} 0.998 & 0.002 \\ 0.003 & 0.997 \end{bmatrix} \tag{6}$$

$$A_{RTT} = \begin{bmatrix} 0.997 & 0.003 \\ 0.004 & 0.996 \end{bmatrix} \tag{7}$$

$$B_{PLR} = \begin{bmatrix} 0.079 & 0.015 & 0.016 & 0.013 & 0.021 & 0.856 \\ 0.607 & 0.076 & 0.055 & 0.038 & 0.026 & 0.196 \end{bmatrix} \tag{8}$$

$$B_{RTT} = \begin{bmatrix} 0.044 & 0.035 & 0.027 & 0.029 & 0.034 & 0.831 \\ 0.528 & 0.092 & 0.046 & 0.029 & 0.030 & 0.275 \end{bmatrix} \tag{9}$$

5 Simulation evaluations

To evaluate the accuracy of introduced HMC reference model, we use it to simulate the HSR wireless network link quality and compare the results to the original measurement result. Normally, a forward induction algorithm can be used to for simulation.

(a) Determine the macro-state of PLR or RTT to be generated by the algorithm at very first step. From the measurement results, we can determine that the initial state of RTT and PLR macro-states are both *poor*, therefore, s_1 is P at first step.

(b) Determine the macro-state of current step based on the macro-state of last step. The probability that the macro-state is j at current step (n), providing that it was i at last step (n-1), can be shown that

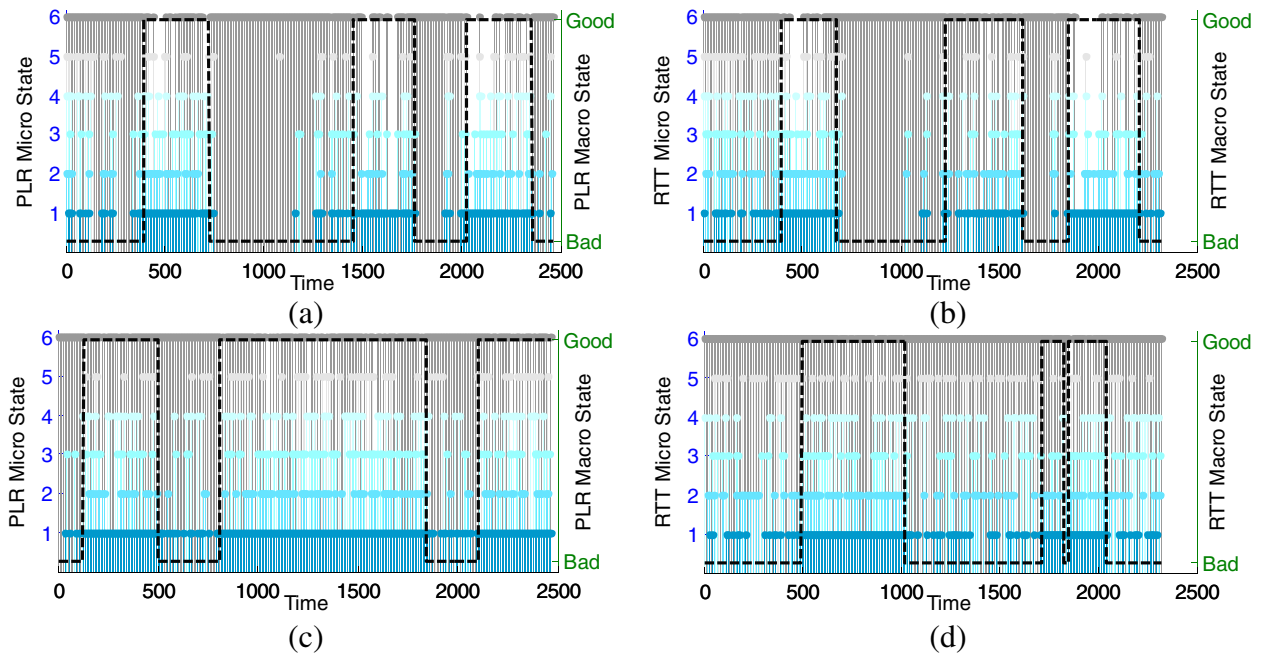

Fig. 6 Simulation results of normal forward induction algorithm. **a** and **b** are the measured macro-states and micro-states of PLR and RTT. **c** and **d** are the simulated macro-states and micro states of PLR and RTT

$$p(s_n = j) = \alpha_{ij},\ i, j \in S \tag{10}$$

Then, select an element from set S randomly according to the probabilities calculated in Eq. 10. This element is the macro-state of current step.

(c) Determine the micro-state based on the macro-state of current step. Presuming at step n the macro-state is j, thus the probability that the micro-state is k at step n is

$$p(q_n = k) = \beta_j(k),\ k \in Q \tag{11}$$

Then, select an element from set Q randomly according the probability calculated in Eq. 11. This element is the micro-state of current step.

(d) Replace n with $n + 1$. Repeat from (b) to (d), until expected total number of steps, which is N, has been executed. N is set as 2466 for simulating PLR, and 2317 for simulating RTT.

A series of cyclical sequence can be simulated by using the normal forward induction algorithm mentioned above. Figure 6 shows a series of simulation results of RTT and PLR, in comparison with the prior measurement results. In this figure, vertical stem lines indicate simulated micro-states. Horizontal dotted lines represent simulated macro-state. Figure 6b and a depict the prior measurement results of RTT and PLR, respectively, while the simulation results of proposed algorithm are shown in Fig. 6c and d. It clearly shows that simulation results possess a cyclical pattern, which is similar to the originally measured value of PLR and RTT. However, the simulation results did not accurately fit the prior measurement results of RTT and PLR, which means that

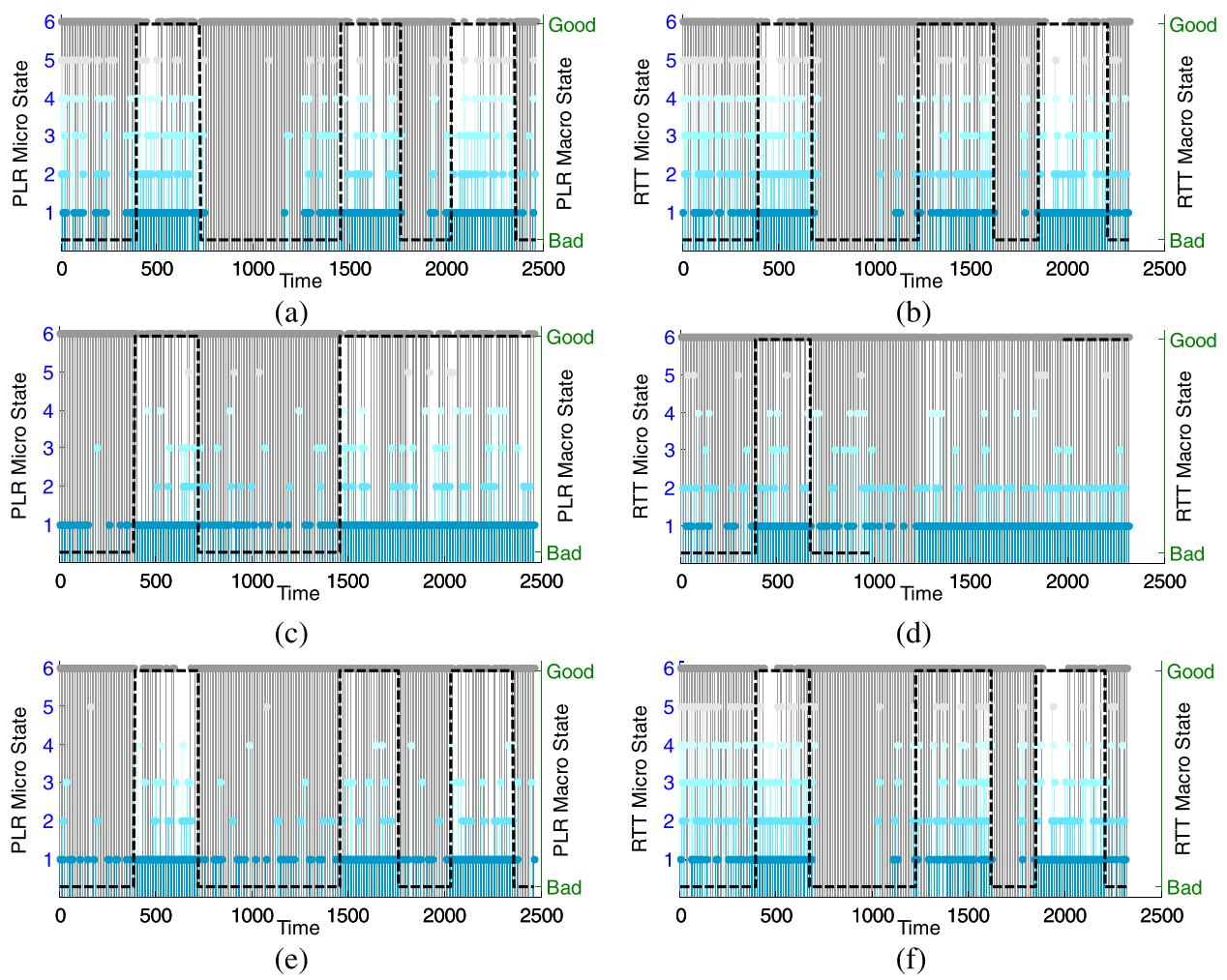

Fig. 7 Simulation results of improved forward induction algorithm. **a** and **b** are the measured macro-states and micro-states of PLR and RTT. **c** and **d** are the simulated macro-states and micro states of PLR and RTT with three probes. **e** and **f** are that with six probes

normal algorithm is unable to accurately simulate HSR wireless network link quality.

The inefficiency of normal forward induction algorithm to accurately simulate HSR link quality stems from the effect of randomness. The accuracy of simulation results is mainly determined by whether the simulated macro-state is correct at step (b) during the forward induction algorithm. If the macro-state fits the prior measurement results, then the accuracy of generated micro-states at step (c) will be greatly improved. However, the macro-state is randomly determined according to the state transition probability A. The randomness makes the macro-state transition uncontrolled.

To tackle this problem, we develop an improved link quality simulation algorithm. Several probes are introduced to *guide* the transition between different macro-states, which would rarely happen. For example, probe n indicates the *nth* simulation step. At *nth* simulation, the macro-state of link quality will be obliged to change, regardless of state transition probability A.

P is the probe set, whose elements are probes selected according to the measurement results. For RTT, P is

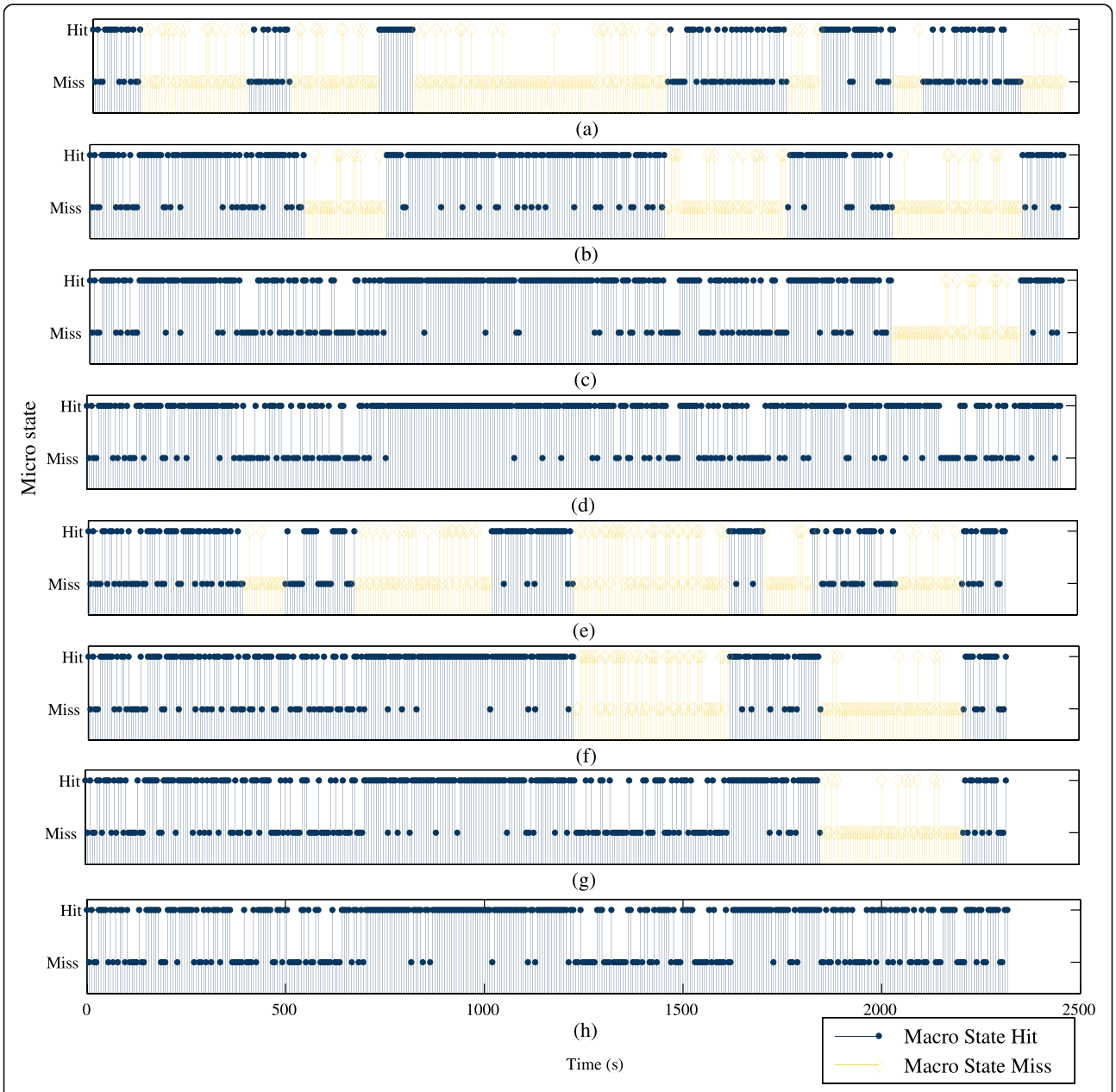

Fig. 8 The hit rates of simulated macro-state and micro-state with 0, 2, 4, 6 probes of PLR (**a** ~ **d**) and RTT (**e** ~ **h**)

{393, 675, 1226, 1617, 1852, 2209}. For PLR, P is {392, 725, 1455, 1763, 2030, 2357}.

When applying probes to guide the transition of macro-state, the determination of macro-state at step (b) in the original algorithm is revised as

$$p(s_n = j) = \begin{cases} \alpha_{ij},\ n \notin p \text{ and } i, j \in S \\ 1,\ n \in p,\ j \neq i,\ \text{and } i, j \in S \\ 0,\ n \in p,\ j = i,\ \text{and } i, j \in S \end{cases} \quad (12)$$

In Fig. 7, the results of improved simulation algorithm are shown in comparison with the measured HSR wireless network link quality. Figure 7a depicts the prior measurement results of PLR. Figure 7c is the simulation result of PLR using improved forward induction algorithm with three probes. When applying three probes, the improved algorithm is able to accurately simulate the top 50% of the prior measured PLR. If six probes are all applied, the second half can also be well simulated, as shown in Fig. 7e. Figure 7b shows the prior measurement results of RTT, Fig. 7d and f show the simulation results of RTT using improved forward induction algorithm applying three probes and six probes. Similar to PLR, more RTT probes applied in the improved algorithm leads to higher accuracy.

To further illustrate how the utilization of probes can make the simulation results better fit measured PLR and RTT, the hit rate of simulated states compared to the measured original states of PLR and RTT is evaluated. In Fig. 8, each stem line represents a simulation step. The hit rate of macro-state is indicated by the line color and marker type while the y coordinate implies the hit rate. Figure 8a ~ d and e ~ h depict the hit rate of simulated PLR and RTT, respectively, using 0 probe, 2 probes, 4 probes, and 6 probes. With more probes used in simulation, the probability that the simulated macro-state hit the corresponding originally measured macro-state becomes higher. Moreover, simulated micro-states are more likely to hit the original ones if the current macro-state is the same as the measured macro-state. This explains why the simulation results match the prior measured PLR and RTT better with more probes used in the simulation.

Figure 9 shows the accuracy of improved link quality simulation algorithm, which rises as the number of probes that are applied increases. The improved algorithm can simulate the micro-state of RTT and PLR with accuracy of 63.5 and 71.2%, when six probes are all applied. Meanwhile, the macro-states of PLR and RTT can be simulated with the accuracy of 100%. Evaluation results prove that the improved link quality simulation algorithm can simulate the measured RTT and PLR with high accuracy, which also proves that the introduced reference model based on HMC is capable of well-reflecting the HSR wireless network link quality.

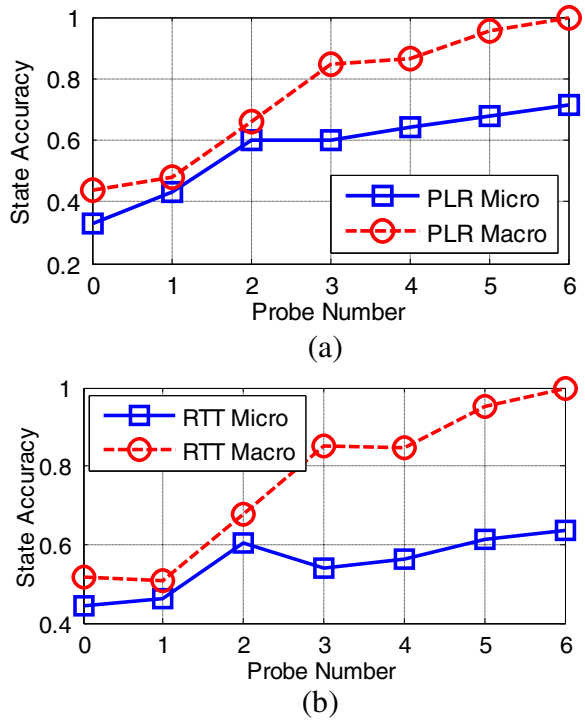

Fig. 9 Relationship between simulation accuracy and probe numbers.

6 Conclusions

In this paper, we firstly conduct a series of field measurement campaigns for PLR and RTT along realistic high-speed rails and gathered a dataset of more than 120000 entries. A cyclical behavior of HSR wireless network link quality is revealed after the investigation of the measurement results. Based on this, we introduce an HMC reference model for describing this cyclical behavior. Also, an improved link quality simulation algorithm is developed. Finally, the assessment of the introduced model and developed simulation algorithm is provided based on simulation experiments. Evaluation results prove that the developed algorithm can reproduce the cyclical behaviors of PLR and RTT with high accuracy. Hence, we conclude that the introduced HMC reference model is valid for HSR wireless network link quality. In the future work, we will further consider the link quality prediction for HSR networks based on our proposed model.

Acknowledgement

This paper is supported by National Basic Research Program of China (973 program) under Grant No. 2013CB329101, National High Technology of China (863program) under Grant No. 2015AA015702, and National Natural Science Foundation of China under Grant No. 61271202.

Competing interests
The authors declare that they have no competing interests.

Received: 31 March 2016 Accepted: 20 October 2016
Published online: 15 November 2016

Reference

1. International Union of Railways, *High Speed*, 2016. http://www.uic.org/highspeed#General-definitions-of-highspeed. Accessed 21 Mar. 2016
2. ETCS/GSM-R quality of service—operational analysis, ERTMS Std. 04E117 (2010)
3. ZM Li, *TD-LTE Boosts the Development of Mobile Broadband*, 2015. http://gtigroup.org/d/file/China%20Mobile%20-%20TD-LTE%20Boosts%20the%20Development%20of%20Mobile%20Broadband.pdf. Accessed 21 Mar 2016
4. HK Zhang, P Dong, W Quan, B Hu, Promoting efficient communications for high-speed railway using smart collaborative networking. IEEE Wireless Commun. **22**(6), 92–97 (2015)
5. B Ai, X Cheng, T Kurner, ZD Zhong, K Guan, RS He, L Xiong, DW Matolak, DG Michelson, CB Rodriguez, Challenges toward wireless communications for high-speed railway. Intell. Transp. Syst. IEEE Trans. **15**(5), 2143–2185 (2014)
6. H Wei, ZD Zhong, KGB Ai, Path loss models in viaduct and plain scenarios of the high-speed railway, in *CHINACOM, 2010 5th International ICST Conference on*, 2010, pp. 1–5
7. RS He, ZD Zhong, B Ai, JW Ding, An empirical path loss model and fading analysis for high-speed railway viaduct scenarios. IEEE Antennas Wireless Propag. Lett. **10**, 808–812 (2011)
8. H Wei, ZD Zhong, L Xiong, B Ai, RS He, Study on the shadow fading characteristics in viaduct scenario of the high-speed railway, in *CHINACOM, 2011 6th International ICST Conference on*, 2011, pp. 1216–1220
9. RS He, ZD Zhong, B Ai, JW Ding, Measurements and analysis of short-term fading behavior for high-speed rail viaduct scenario, in *Communications (ICC), 2012 IEEE International Conference on*, 2012, pp. 4563–4567
10. RS He, ZD Zhong, B Ai, GP Wang, JW Ding, AF Molisch, Measurements and analysis of propagation channels in high-speed railway viaducts. Wireless Commun. IEEE Trans. **12**(2), 794–805 (2013)
11. T Zhou, C Tao, S Salous, ZH Tan, L Liu, L Tian, Graph-based stochastic model for high-speed railway cutting scenarios. IET Mircow. Antennas Propag. **9**(15), 1691–1697 (2015)
12. L Tian, J Zhang, C Pan, Small scale fading characteristics of wideband radio channel in the u-shape cutting of high-speed railway, in *Vehicular Technology Conference (VTC Fall), 2013 IEEE*, 2013, pp. 1–6
13. B Chen, Z Zhong, B Ai, DG Michelson, A geometry-based stochastic channel model for high-speed railway cutting scenarios. IEEE Antennas Wireless Propag. Lett. **2015**(14), 851–854 (2015)
14. RS He, ZD Zhong, B Ai, JW Ding, Y Yang, AF Molisch, Short-term fading behavior in high-speed railway cutting scenario: measurements, analysis, and statistical models. Antennas Propag. IEEE Trans. **61**(4), 2209–2222 (2013)
15. RS He, ZD Zhong, B Ai, JW Ding, Propagation measurements and analysis for high-speed railway cutting scenario. Electron. Lett. **2011**(47), 1167–1168 (2011)
16. RS He, ZD Zhong, B Ai, JW Ding, Y Yang, Propagation measurements and analysis of fading behavior for high speed rail cutting scenarios, in *Global Communications Conference (GLOBECOM), 2012 IEEE*, 2012, pp. 5015–5020
17. K Guan, ZD Zhong, B Ai, RS He, C Briso, Five-zone propagation model for large-size vehicles inside tunnels. Progr. Electromagn. Res. **138**, 389–405 (2013)
18. K Guan, ZD Zhong, B Ai, T Kurner, Propagation measurements and modeling of crossing bridges on high-speed railway at 930 MHz. Veh. Technol. IEEE Trans. **63**(2), 502–517 (2014)
19. K Guan, ZD Zhong, B Ai, T Kurner, Propagation measurements and analysis for train stations of high-speed railway at 930 MHz. Veh. Technol. IEEE Trans. **63**(8), 3499–3516 (2014)
20. JH Qiu, C Tao, L Liu, ZH Tan, Broadband channel measurement for the high-speed railway based on WCDMA, in *Vehicular Technology Conference (VTC Fall), 2012 IEEE*, 2012, pp. 1–5
21. MQW RJ Zhao, X Xiang, JQ Yang, Measurement and modeling of the LTE train-ground channel for high-speed railway in viaduct scenario, in *Vehicular Technology Conference (VTC Fall), 2014 IEEE*, 2014, pp. 1–5
22. CU Bas, SC Ergen, Spatio-temporal characteristics of link quality in wireless sensor networks, in *Wireless Communications and Networking Conference (WCNC), 2012 IEEE*, 2012, pp. 1152–1157
23. H Hoeller, C Reinke, J Neumann, S Grope, F Frischat, V Linnemann, Information quality model and optimization for 802.15.4-based wireless sensor networks. J. Netw. Comput. Appl **34**(6), 1773–1783 (2011)
24. F Song, Y Zhang, The Correlation Study for Parameters in Four Tuples. Int. J. Ad Hoc Ubiq. Co. **19**(1/2), 38–49 (2015)
25. MEM Campista, PM Esposito, IM Moraes, C LHMk, D OCMb, DG Passos, CVND Albuquerque, DCM Saade, MG Rubinstein, Routing metrics and protocols for wireless mesh networks. IEEE Network **22**(1), 6–12 (2008)
26. J Santa, PJ Fernández, F Pereñíguez, AF Skarmeta, Real experience with IPv6 communications in highways. J. Wireless Mobile Netw. Ubiquitous Comput. Dependable Appl. **6**(3), 36–53 (2015)
27. F Song, R Li, Feasibility and issues for establishing network-based carpooling scheme. Pervasive Mob. Comput. **24**, 4–15 (2015)
28. DG Jiménez, F Le Gall, Testing a commercial sensor platform for wideband applications based on the 802.15.4 standard. J. Wireless Mobile Netw. Ubiquitous Comput. Dependable Appl **6**(1), 24–36 (2015)
29. F Song, D Huang, An optimization-based scheme for efficient virtual machine placement. Int. J. Parallel Prog. **42**(5), 853–872 (2014)
30. M Devipriya, B Nithya, C Mala, Hashing based distributed backoff (HBDB) mechanism for IEEE 802.11 wireless networks. J. Internet Services Inf. Security **5**(3), 1–18 (2015)
31. F Song, The throughput critical condition study for reliable multipath transport. Comput. Sci. Inf. Syst. **10**(2), 567–587 (2013)
32. N Oliveira, A Silva, LS Barbosa, IMCReo: interactive Markov chains for stochastic Reo. J. Internet Services Inf. Security **5**(1), 3–28 (2015)